A New Species of Microtegu Lizard (Gymnophthalmidae: Cercosaurinae) from Amazonian Ecuador

Authors: Torres-Carvajal, Omar, Parra, Vanessa, Sales Nunes, Pedro M., and Koch, Claudia

Source: Journal of Herpetology, 55(4) : 385-395

Published By: Society for the Study of Amphibians and Reptiles

URL: https://doi.org/10.1670/20-142

Journal of Herpetology, Vol. 55, No. 4, 385–395, 2021

A New Species of Microtegu Lizard (Gymnophthalmidae: Cercosaurinae) from Amazonian Ecuador

Omar Torres-Carvajal,[1,4] Vanessa Parra,[1] Pedro M. Sales Nunes,[2] and Claudia Koch[3]

[1]*Museo de Zoología, Escuela de Ciencias Biológicas, Pontificia Universidad Católica del Ecuador, Avenida 12 de Octubre 1076 y Roca, Quito, Ecuador*
[2]*Departamento de Zoologia, Centro de Biociências, Universidade Federal de Pernambuco, Avenida Professor Moraes Rego, s/n. Cidade Universitária CEP 50670-901, Recife, PE, Brazil*
[3]*Zoologisches Forschungsmuseum Alexander Koenig, Adenauerallee 160, 53113 Bonn, Germany*

Abstract.—We describe a new species of Microtegu lizard (*Selvasaura*) from the Amazonian slopes of the Andes in Ecuador. Among other characters, the new species differs from the only other known species of *Selvasaura*, namely, *Selvasaura brava* from Peru, in having more femoral pores in males and a unilobed hemipenis. We present the first description of the skull of *Selvasaura*, along with a molecular phylogeny of Cercosaurinae and genetic distances as additional evidence supporting delimitation of the new species.

Resumen.—Describimos una especie nueva de lagartija microtegu (*Selvasaura*) de las estribaciones amazónicas de los Andes del Ecuador. Aparte de otras características, la especie nueva difiere de la única otra especie conocida de *Selvasaura*, *Selvasaura brava* del Perú, por poseer más poros femorales en los machos y un hemipene unilobado. Presentamos por primera vez la descripción del cráneo de *Selvasaura*, junto con una filogenia molecular de Cercosaurinae y distancias genéticas como evidencia adicional para la delimitación de la especie nueva.

In this century, systematic studies of Neotropical lizards have focused strongly on Gymnophthalmidae, one of the most diverse lizard taxa from southern Mexico to Argentina and the Caribbean. Phylogeny-based taxonomic rearrangements and descriptions of new species and genera of gymnophthalmid lizards are common in recent herpetological literature (Goicoechea et al., 2016; Torres-Carvajal et al., 2016; Moravec et al., 2018; Sánchez-Pacheco et al., 2018; Lehr et al., 2019; Fang et al., 2020; Recoder et al., 2020; Vásquez-Restrepo et al., 2020). Nearly one-third of the ~265 known species of Gymnophthalmidae (Uetz et al., 2020) have been described since the beginning of the 21st century, when the first comprehensive molecular phylogenies of this clade were published (Pellegrino et al., 2001; Castoe et al., 2004).

About half of the species of Gymnophthalmidae is nested within the clade Cercosaurinae Gray 1838. In a comprehensive molecular phylogenetic study of Cercosaurinae lizards, Torres-Carvajal et al. (2016) recovered three clades that could not be assigned to any of the genera recognized at the time. One of them (unnamed clade 1) was subsequently recognized as *Euspondylus* (Chávez et al., 2017), whereas another (unnamed clade 3) was described as a new genus, *Selvasaura* Moravec et al. 2018, occurring along the Amazonian slopes of the Andes from northern Ecuador to southern Peru. To date, only the type species *Selvasaura brava* Moravec et al. 2018, the Brave Forest Microtegus, has been described from the Junín region in southern Peru. Here, we describe a species of *Selvasaura* from Ecuador based on molecular and morphological evidence and present the first description of the skull of this genus.

Materials and Methods

Measurements and Lepidosis.—Specimens of the new species described here were collected during several field trips to different localities in Amazonian Ecuador between 2008–2014. Altitudes and geographic coordinates were recorded with a GPS (Garmin) by using the geodetic datum WGS84. After lethal anesthetization of voucher specimens with an intracelomic injection of benzocaine (2%), muscle and liver tissue samples were extracted for DNA analyses. Specimens were then fixed in 10% formalin and stored in 70% ethanol at Museo de Zoología, Pontificia Universidad Católica del Ecuador, Quito (QCAZ). The following measurements were taken with a digital caliper to the nearest 0.1 mm: snout–vent length (SVL), tail length (TL), head length (HL) from anterior border of tympanum to tip of snout, maximum head width (HW), maximum head depth (HD), eye–snout distance (EN) from anterior corner of eye to tip of snout, forelimb length (FLL) from limb insertion to tip of fourth finger, hindlimb length (HLL) from limb insertion to tip of fourth toe, and axilla–groin distance (AGD). In addition, we recorded characters of lepidosis following previous works (Montanucci, 1973; Parra et al., 2020).

Osteology.—Osteological description of the skull of the holotype of the species of *Selvasaura* presented in this paper is based on a high-resolution micro-computed tomography (CT) scan, performed with a Bruker SkyScan 1173 instrument at the University of Toronto (Toronto, Canada). The scan was conducted with an X-ray beam at 47-kV source voltage and 170-μA current without the use of a filter. Rotation steps of 0.2° were used with a frame average of 2, recorded over a 180° rotation, resulting in 1,200 projections of 950-ms exposure time each and a total scan duration of 38:40 min. The magnification setup generated data with an isotropic voxel size of 9.96 μm. The CT dataset was reconstructed using N-Recon software version 1.7.1.6 (Bruker MicroCT) and rendered in three dimensions through the aid of Amira visualization software (FEI, Thermo Fisher Scientific). Amira was further used for segmentation to separate individual bones and highlight them in different colors. No bone sutures were visible between prootic and otoccipital and between the surangular and articular/prearticular complex. Cartilage structures were omitted from the osteological descriptions because cartilage is hardly visible in the unstained micro-CT scan. Osteological terminology follows Torres-Carvajal (2003) and Evans (2008).

Hemipenial Morphology.—The left hemipenis of the male paratype QCAZ 5073 was prepared following the procedures

[4]Corresponding author. E-mail: omartorcar@gmail.com
DOI: 10.1670/20-142

described by Manzani and Abe (1988), modified by Pesantes (1994) and Zaher (1999). The organ was everted after immersion in a potassium hydroxide solution. The retractor muscle was manually separated, and the everted organ was filled with stained petroleum jelly. The organ was then immersed in an alcoholic solution of Alizarin red for 24 h to stain eventual calcified structures (e.g., spines or spicules), in an adaptation proposed by Nunes et al. (2012) on the procedures described by Uzzell (1973) and Harvey and Embert (2008). The terminology of hemipenial structures follows previous literature (Nunes et al., 2012).

Phylogenetic Analyses.—Nucleotide sequences of three mitochondrial genes, namely, ribosomal small (12S) and large (16S) subunit genes and subunit IV of NADH dehydrogenase (ND4), as well as one nuclear gene, namely, oocyte maturation factor MOS (c-mos), were used in a recent comprehensive phylogenetic study of Cercosaurinae (Torres-Carvajal et al., 2016). Following the same laboratory and alignment protocols, we obtained new gene sequences from two specimens of the new species described here. We added to our dataset sequences from GenBank by selecting one sample per species of all clades ranked as genera within Cercosaurinae except *Selvasaura*, for which we retrieved all available samples including one sample of the new species (QCAZ12798). We also added 27 samples of undescribed taxa, such as "unnamed clade 2." For species with multiple GenBank specimen vouchers, we selected the voucher with the largest gene coverage and least missing data. Our data matrix contained 1,949 characters and 147 terminals representing 103 currently recognized species of Cercosaurinae and seven outgroup taxa (Supplementary Table 1). Trees were rooted with *Alopoglossus* (Pellegrino et al., 2001; Castoe et al., 2004; Goicoechea et al., 2016).

The best-fit nucleotide substitution models and partitioning scheme were chosen simultaneously using PartitionFinder v2.1.1 (Lanfear et al., 2012) under the Bayesian Information Criterion (BIC). Genes were combined into a single dataset, and the "greedy" algorithm was used with branch lengths of alternative partitions "linked" to search for the best-fit scheme. Both maximum likelihood (ML) and Bayesian inference (BI) methods were used to obtain the optimal tree topology of the combined, partitioned dataset by using the programs RAxML-HPC2 v8.2.12 (Stamatakis, 2014) and MrBayes v3.2.6 (Ronquist et al., 2012), respectively. The ML analysis was performed under the GTRGAMMA model for all partitions. Nodal bootstrap support (BS) was assessed with the rapid bootstrapping algorithm and 1,000 replicates. Regarding the Bayesian analysis, four independent analyses were performed, each consisting of 10^7 generations and four Markov chains with default heating values. Trees were sampled every 10,000 generations. Results were analyzed in MrBayes and Tracer 1.7 (Rambaut et al., 2018) to assess convergence and effective sample sizes (values >200) for all parameters, based on which the first 10% of trees were removed from each run. The remaining trees were used to calculate posterior probabilities (PP) for each bipartition in a majority-rule consensus tree. The phylogenetic trees were visualized and edited using FigTree v1.4.4 (Rambaut, 2018). Additionally, uncorrected genetic distances between *Selvasaura brava* and the new species described below were calculated in MEGA (Kumar et al. 2016) for 12S and 16S.

Results

The taxonomic conclusions of this study are based on the study of external morphology and color pattern, as well as inferred phylogenetic divergences. We consider this information as species delimitation criteria following the unified species concept (de Queiroz, 2007).

FIG. 1. Holotype (QCAZ 12798; SVL = 39.54 mm) of *Selvasaura almendarizae* sp. nov. in dorsal (top) and ventral (bottom) views. Photographs by J. Carrión.

Selvasaura ***almendarizae*** sp. nov.
Figs. 1–7

Unnamed clade 3 (Torres-Carvajal et al., 2016) in part.
Selvasaura sp. (Moravec et al., 2018) in part.
Proposed standard English name: Almendáriz's Microtegus
Proposed standard Spanish name: Microtegúes de Almendáriz

Holotype.—QCAZ 12798 (Figs. 1, 2), adult male, Ecuador, Provincia Napo, Wildsumaco Wildlife Sanctuary, 0°41′17.17″S, 77°36′1.45″W, WGS84, 1,350 m, 22 July 2014, collected by J. Camper.

Paratypes (2).—ECUADOR: Provincia Napo: QCAZ 5073, adult male, same collection data as holotype except 0°40′46.96″S, 77°36′2.81″W, 1,250 m, 30 July 2012. Provincia Pastaza: QCAZ 9140, adult male, Zanjarajuno Ecological Center, 1°22′19.08″S, 77°51′57.99″W, 940 m, 20 March 2008, collected by P. Rivera, L. Coloma, and S. Ron.

Diagnosis.—The new species belongs to *Selvasaura* as defined by Moravec et al. (2018). However, in the absence of morphological synapomorphies defining *Selvasaura*, the new species is assigned to *Selvasaura* based on phylogenetic evidence (Fig. 8; see also Moravec et al., 2018). *Selvasaura almendarizae* sp. nov. differs from *S. brava* (Table 1) in having more femoral pores in males (9–12 vs. 7–9, respectively), fewer gular collar scales (7–9 vs. 9–11), fewer transverse rows of dorsals (25–32 vs. 33–36), fewer scales around midbody (29–32 vs. 32–34), and fewer lateral scale rows (5 vs. 6–7). The new taxon can be further distinguished from *S.*

FIG. 2. Head of the holotype (QCAZ 12798) of *Selvasaura almendarizae* sp. nov. in dorsal (top), lateral (middle), and ventral (bottom) views. Individual scales were traced for clarity. Photographs by J. Carrión.

brava and other Cercosaurinae species in having a unilobed hemipenis, which among microteiids has been reported only in a few species within Gymnophthalminae (*Calyptommatus* sp., *Nothobachia ablephara*, and *Scriptosaura catimbau*) and Alopoglossidae (*Alopoglossus brevifrontalis*, *Alopoglossus festae*, *Alopoglossus kugleri*, *Alopoglossus myersi*, and *Alopoglossus plicatus*; Nunes, 2011; Hernández Morales et al., 2020).

Characterization.—(1) Three to four supraoculars, anteriormost larger than posterior one; (2) two prefrontals; (3) 9–12 femoral pores in males (females unknown); (4) lower eyelid scale single and transparent; (5) scales on dorsal surface striated; (6) five rows of lateral scales at midbody; (7) 25–32 dorsal scales between occipital and posterior margin of hindlimb; (8) lateral body fold present; (9) keeled ventrolateral scales on each side absent; (10) dorsum brown with a conspicuous, cream or gray vertebral stripe with wavy borders and scattered black marks along sides, extending from interparietal or postparietal to tip of tail; (11) white labial stripe present, with black outline on dorsal border and brown flecks or brown transversal bars on supralabials; (12) flanks of body grayish brown, turning cream on ventrolateral region; (13) white stripe along forelimb absent; (14) adult males with a longitudinal row of ocelli (black thick outline and white center) extending from above forelimb insertion posteriorly along flanks.

Description of Holotype.—Adult male (QCAZ 12798); SVL 39.54 mm; TL 73.04 mm; HL 9.65 mm; HW 5.3 mm; HD 3.92 mm; EN 3.38 mm; FLL 13.31 mm; HLL 18.61 mm; AGD 19.11 mm.

Dorsal and lateral head scales smooth, juxtaposed; rostral subrectangular, 1.43 times wider than high; frontonasal pentagonal, laterally in contact with nasal, smaller than frontal; prefrontals hexagonal, longer than wide, with medial suture, laterally in contact with nasal, loreal, and first superciliary; frontal hexagonal, longer than wide, wider anteriorly, in contact with prefrontals and supraoculars I and II; frontoparietals pentagonal, longer than wide, wider posteriorly, each in lateral contact with supraoculars II and III; interparietal heptagonal, lateral borders parallel to each other; parietals slightly shorter than interparietal, polygonal, positioned anterolaterally to interparietal, each in lateral contact with supraocular III and dorsalmost postocular; postparietals three, medial scale smaller than laterals; supralabials seven, fourth slightly longer and below center of eye; infralabials seven, fourth below center of eye; temporal enlarged, juxtaposed, smooth, polygonal; one enlarged, smooth supratemporal; nasal divided above and below nostril, subtriangular, wider than long, in contact with rostral anteriorly, supralabials I and II ventrally, frontonasal and prefrontals dorsally, loreal posterodorsally and frenocular posteroventrally; loreal rectangular; frenocular trapezoidal, in contact with nasal, separating loreal from supralabials; supraoculars three, first one largest; 4/5 (right/left) superciliaries, first one enlarged, extending onto dorsal surface and in contact with loreal; palpebral disk single, transparent; three suboculars, third one largest; three postoculars of similar size; ear opening round, without denticulate margins; tympanum recessed into a shallow auditory meatus; mental 1.27 times wider than long; postmental pentagonal, wider than long, followed posteriorly by four pairs of genials, anterior two in contact medially, posterior two separated by postgenials; all genials in contact with infralabials; gulars imbricate, smooth, in nine rows; gular fold complete; posterior row of gulars (collar) with nine scales that are similar to each other in size medially and become smaller laterally.

Scales on nape wider than those of dorsals; scales on sides of neck small and granular; dorsal scales elongated, imbricate, arranged in transverse rows; scales on dorsal surface of neck striated; 28 dorsals between occiput and posterior margin of hindlimbs; 16 dorsal scale rows in a transverse line at midbody; ventrolateral scales smooth; dorsals separated from ventrals by five rows of small scales at level of 13th row of ventrals; lateral body fold present; ventrals smooth, wider than long, arranged in 23 transverse rows between collar fold and preanals; 10 ventral scale rows in a transverse line at midbody; subcaudals smooth; limbs overlapping when adpressed against body; axillary region with granular scales; scales on dorsal surface of forelimb smooth, imbricate; scales on ventral surface of forelimb granular; 3 thick, smooth thenar scales; supradigitals 4/4 (right/left) on finger I, 6/6 on II, 8/8 on III, 9/9 on IV, 6/6 on V; supradigitals 4/4 on toe I, 7/7 on II, 9/9 on III, 11/12 on IV, 9/8 on V; subdigital lamellae of forelimb single, 6/7 on finger I, 12/11 on II, 14/13 on III, 14/12 on IV, 11/10 on V; subdigital lamellae on toe I single, divided on toes II-V from half-length to base, 6/- on toe I, 11/11 on II, 15/16 on III, 20/20 on IV, 14/13 on V; groin region with small, imbricate scales; scales on dorsal surface of hindlimbs smooth, imbricate; scales on ventral

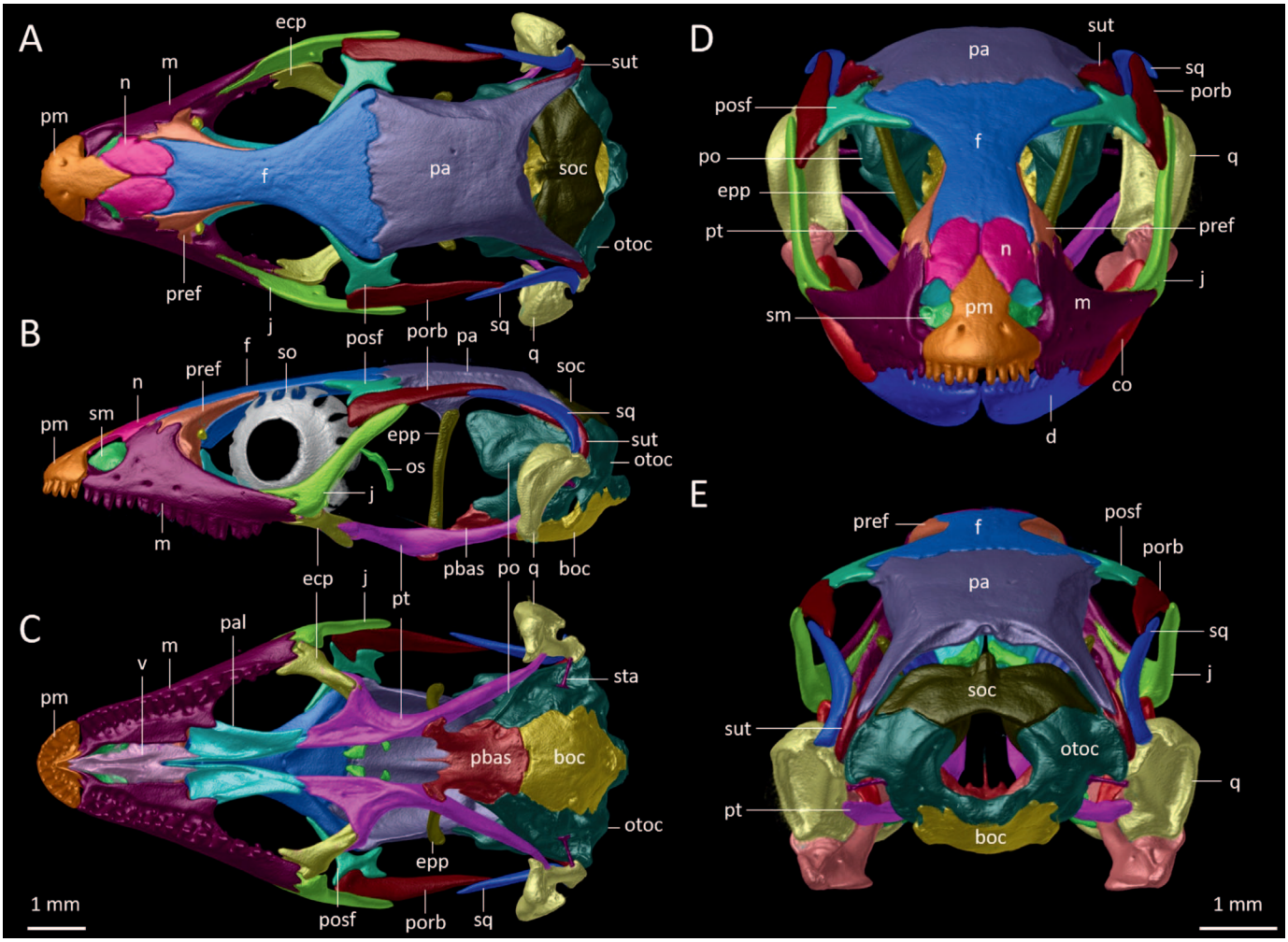

FIG. 3. Skull of the holotype of *Selvasaura almendarizae* sp. nov. (QCAZ 12798) in (A) dorsal, (B) lateral, (C) ventral, (D) anterior, and (E) posterior views. Abbreviations: boc, basioccipital; ecp, ectopterygoid; epp, epipterygoid; f, frontal; j, jugal; m, maxilla; n, nasal; os, orbitosphenoid; otoc, otoccipital; pa, parietal; pbas, parabasisphenoid; pal, palatine; pm, premaxilla; po, prootic; porb, postorbital; posf, postfrontal; pref, prefrontal; pt, pterygoid; q, quadrate; sm, septomaxilla; soc, supraoccipital; sq, squamosal; sta, stapes; sut, supratemporal; v, vomer. Images by C. Koch. Scale bars correspond to left and right images, respectively.

surface of hindlimbs smooth; scales on posterior surface of hindlimbs granular; 12/11 femoral pores on each leg; preanal pores absent; cloacal plate with four scales, bordered by four scales anteriorly, of which the two medial-most are enlarged.

Cranial Osteology of Holotype.—The skull of *Selvasaura almendarizae* sp. nov. (Figs. 3, 4) is depressed (skull height = 46% of skull length) and moderately long (skull width = 51% of skull length). Marginal teeth are present on the maxillary arcade (i.e., premaxilla and maxillae) and palatal teeth are absent. The opisthotics-exoccipitals and parasphenoid-basisphenoid are indistinguishably fused and, therefore, are described as single units, namely, otoccipitals and parabasisphenoid, respectively. The mandible is dentigerous and V-shaped in dorsal and ventral profiles, and its greatest width is approximately 13% of its total length (Fig. 5). Each mandibular ramus increases slightly in height posteriorly and has approximately the same width throughout its length. The rami meet anteriorly forming the mandibular symphysis.

Dermatocranium: The premaxilla forms the anteromedial margin of the snout and the medial margin of each fenestra exonarina. It bears a broad posterodorsally oriented nasal process, which extends and tapers between the anterior half of the nasals, and a broader anterior alveolar portion. The premaxilla articulates with the maxillae anterolaterally and the nasals posteriorly. The tapered posterior end of the nasal process articulates with the anteromedial margins of the nasals. In ventral view, the premaxilla bears a chevron-shaped medial ridge pointing forward and extending halfway the length of the premaxilla. The ventral surface of the premaxilla lacks posteroventral extensions at its articulation with the maxilla. Anteroventrally, the alveolar portion of the premaxilla bears 10 conical teeth.

The septomaxillae are dorsoventrally compressed and lie anteromedially within the nasal capsules, lateral to the nasal septum. They form the floor of the anteromedial portion of the nasal cavity and the roof of the cavum containing the vomeronasal organ. The septomaxillae are oriented anteroventrally and articulate with the maxillae anterolaterally and the vomers ventrally.

The maxillae occupy most of the anterolateral aspect of the skull between the orbits and the snout. In lateral aspect, each maxilla extends approximately 38% the length of the skull. Each maxilla bears 14 laterally compressed teeth on a well-developed alveolar shelf. Maxillary dentition is heterodont, with conical

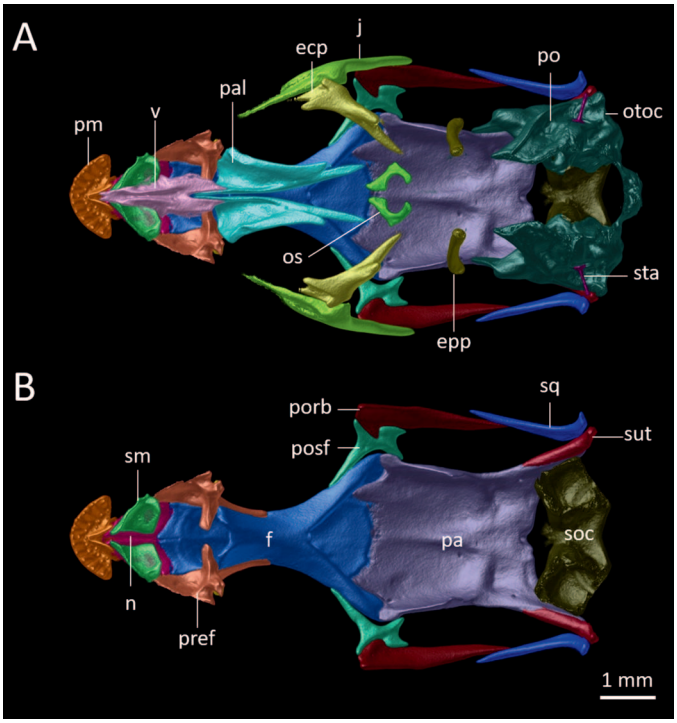

FIG. 4. Skull of the holotype of *Selvasaura almendarizae* sp. nov. (QCAZ 12798) in ventral view after sequential removal of (A) maxillae, pterygoids, quadrates, parabasisphenoid, and basioccipital; and (B) vomers, palatines, jugals, ectopterygoids, orbitosphenoids, epipterygoids, otoccipitals, prootics, and stapes. Abbreviations are the same as those in Fig. 3. Images by C. Koch.

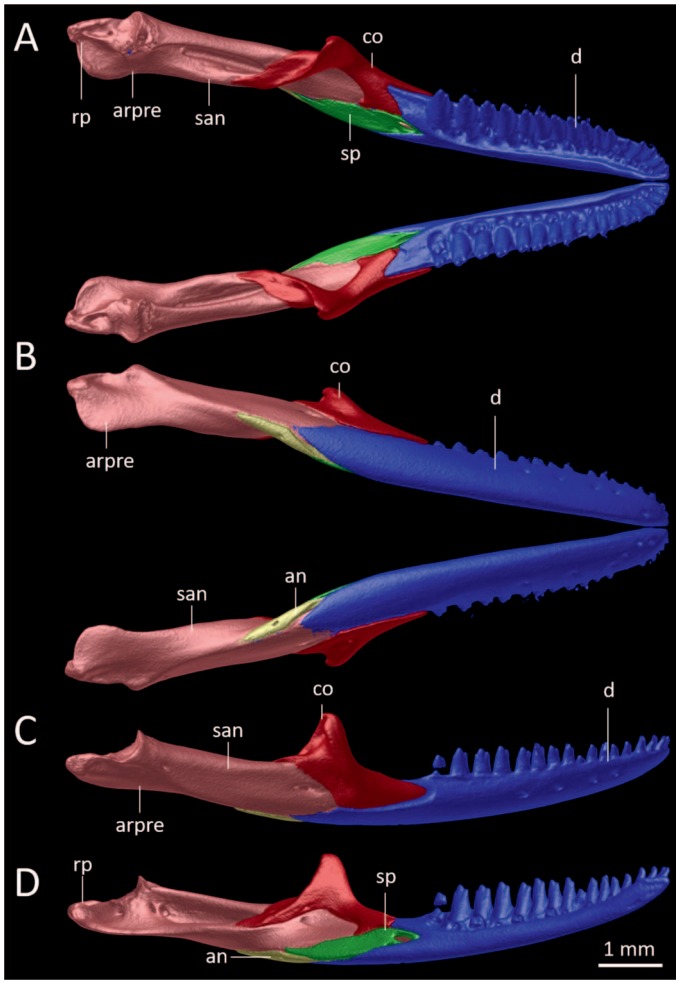

FIG. 5. Mandible of the holotype of *Selvasaura almendarizae* sp. nov. (QCAZ 12798) in (A) dorsal, (B) ventral, (C) lateral, and (D) medial views. Abbreviations: an, angular; arpre, articular/prearticular complex (fused with surangular); co, coronoid; d, dentary; rp, retroarticular process; san, surangular; sp, splenial. Images by C. Koch.

anterior teeth and larger, tricuspid (lateral cusps much smaller than the medial one) posterior teeth. In an anterior-to-posterior sequence in lateral view, the maxilla articulates with the premaxilla, nasal, prefrontal, jugal, and ectopterygoid. The preorbital facial process of each maxilla forms the lateral rim of the fenestra exonarina. There are three anterior inferior alveolar foramina on the pars facialis of the maxilla. The posterior half of the pars facialis of each maxilla extends to a point posterior to the center of the orbit and overlaps the jugal. The part of the maxilla bearing the last four teeth forms part of the floor of the orbit, as well as the anterolateral rim of the inferior orbital fenestra. The maxillae articulate with the jugals posterodorsally and ectopterygoids posteroventrally. In ventral view, the anterior half of each maxillary alveolar shelf is expanded medially and overlaps the corresponding vomer laterally; this expansion makes the medial borders of the shelves parallel to each other. Posteriorly, each alveolar shelf bears a triangular medial process that overlaps the anterolateral aspect of each palatine. In posterior view, the dorsal aspect of each maxilla is notched at a point about halfway its length to form the floor of the maxillopalatine foramen.

The nasals form most of the roof of the nasal capsules. They articulate with the nasal process of the premaxilla anteriorly and overlap the frontal posteriorly. The internasal suture represents approximately half the length of each nasal. In an anterior-to-posterior sequence, the lateral margin of each nasal articulates with the maxilla, prefrontal, and frontal, respectively. The nasal-prefrontal articulation is interrupted posteriorly by the slender anterolateral processes of the frontal. Anteriorly, the nasal forms the posterodorsal rim of the fenestra exonarina. The prefrontals form the anterodorsal rims of the orbits. Each prefrontal articulates with the nasal and frontal dorsally and with the maxilla anteriorly, ventrolaterally, and ventrally. In posterior view, the ventral margin of each prefrontal is notched to form the roof of the maxillopalatine foramen. The lacrimals are absent.

The frontal lies between the orbits, is longer than wide, and forms most of the dorsal orbital margin. Anteriorly, the frontal is W-shaped in dorsal view because it is partially overlapped by the nasals. In ventral view, the anterolateral processes are shorter than the anteromedial process. The anterolateral processes articulate with the dorsal margin of the prefrontals. The transverse posterior margin of the frontal lies posterior to the orbits and articulates with the anterior margin of the parietal. Posterolaterally, the frontal articulates with the anterior third of the anterior process of the postfrontal. In ventral view, the cristae cranii are strongly developed and meet anteriorly to form a tubular structure.

The parietal forms most of the posterior surface of the skull table. Laterally, the parietal extends ventrally and forms the medial rim of the supratemporal fossae. Posteriorly, the corpus of the parietal bears a pair of long supratemporal processes that are laterally overlapped by the supratemporals, which are laterally compressed and extend anteriorly less than half the

FIG. 6. Specimens of *Selvasaura almendarizae* sp. nov. in life. (A, B) paratype QCAZ 9140, SVL = 39.73 mm; (C, D) uncollected specimens from Bigal River Biological Reserve, Napo Province (see map in Fig. 9). Photographs by S. R. Ron (A, B), A. Anker (C), and T. Garcia (D).

length of the supratemporal fossa. The distal end of each supratemporal process approaches the paraoccipital process of the otoccipital. Medially, the posteroventral surface of the parietal bears the parietal fossa.

The postfrontals are small, flat, star-shaped bones that form part of the posterodorsal rims of the orbits. Each postfrontal has a long anterior process that articulates with the frontal anteromedially and three short posterior processes. The postfrontals articulate with the postorbitals laterally.

The postorbitals are long, flat, wider anteriorly and form the posterolateral margins of the skull along with the squamosals. The postorbitals lie ventral to the postfrontals, forming part of the posterodorsal rim of the orbits. The posterior end of each postfrontal articulates with the medial face of the squamosal.

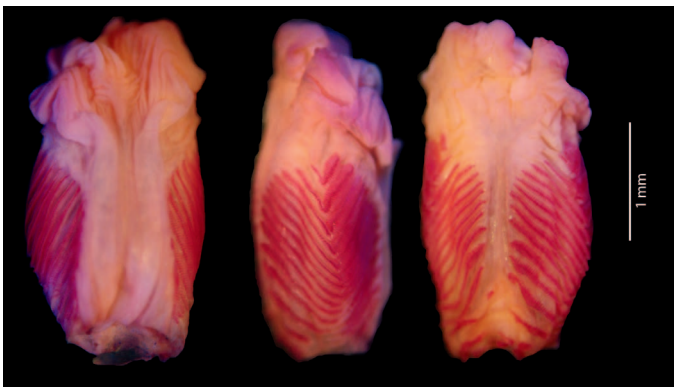

FIG. 7. Hemipenis of *Selvasaura almendarizae* sp. nov. (QCAZ 5073, paratype) in sulcate (left), lateral (middle), and asulcate (right) views. Photographs by P. M. S. Nunes.

The squamosals are slender and crescent-shaped and form the posterolateral rims of the supratemporal fossae and the posterior halves of the supratemporal arches. Posteriorly, the squamosal articulates dorsally with the posterior end of the supratemporal and ventrally with the cephalic condyle of the quadrate.

Jugals are broadly V-shaped and largely overlapped by the maxillae anterolaterally, forming the posteroventral rims of the orbits. Each jugal is composed of two elongate processes that enclose an obtuse angle, with the vertex lying approximately halfway between the anterior and posterior ends of the skull. The anterior or maxillary process articulates with the maxilla anteriorly, ventrally, and laterally and ectopterygoid posteromedially. The dorsal third of the posterior or temporal process of the jugal articulates with the postorbital.

Vomers are the most anterior elements of the palate and form the medial border of each fenestra vomeronasalis externa anteriorly and each fenestra exochoanalis posteriorly. The vomers are fused medially along the anterior two-thirds of their length; the anterior end is tapered and V-shaped and overlaps the posteroventral aspect of the premaxilla. Ventrally, the fused vomers bear two conspicuous ridges that are arched toward each other.

Palatines are medially separated by the anterior half of the pyriform space. Each palatine is widest anteriorly; the tapered posterior end contacts the pterygoid. Anteriorly, the palatines overlap the vomers dorsally, thereby lying in the most dorsal aspect of the palate. Ventrally, each palatine bears a deep concavity, which represents the choanal duct extending from the

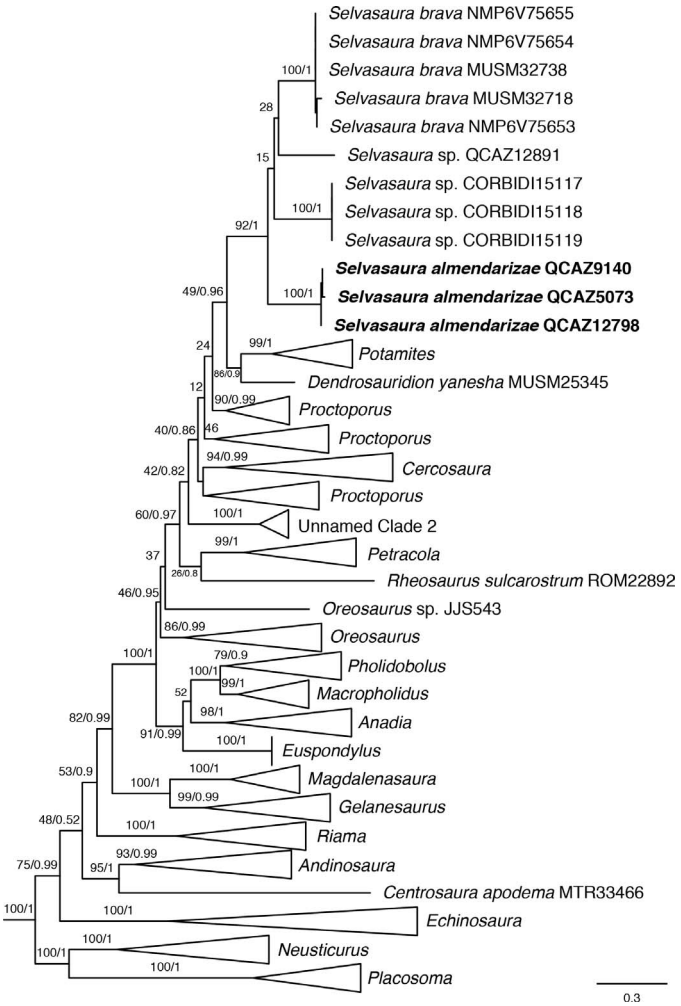

FIG. 8. Phylogeny of Cercosaurinae. Maximum likelihood tree obtained under a RAxML analysis of 147 taxa and 1,949 aligned base pairs of mitochondrial and nuclear DNA. Bootstrap support values/posterior probabilities are indicated next to branches. Except for *Selvasaura*, clades ranked as genera were collapsed into triangles if two or more species were included. Outgroup taxa are not shown. Bayesian and RAxML tree files are provided as Supplementary Tree Files 1, 2.

choanal opening anteriorly. A conspicuous pterygoid process descends ventrally and forms the anteromedial margin of the inferior orbital fenestra.

The ectopterygoids form the posterolateral rims of the inferior orbital fenestrae. Each ectopterygoid bears three processes, namely, anterior, lateral, and posterior processes. The anterior process overlaps the posterior end of the maxilla, whereas the lateral process contacts the jugal. The posterior process is forked and braces the distal end of the transverse process of the pterygoid.

The pterygoids are the largest and most posterior elements of the palate. They form the posteromedial rim of each inferior orbital fenestra and, together with the parabasisphenoid, the rim of the posterior half of the pyriform space. Anteriorly, each pterygoid bears a palatine process medially and a transverse process laterally. Each flat palatine process is overlapped dorsally by the pterygoid process of each palatine. Each transverse process extends laterally, and its distal end is embraced by the dorsal and ventral branches of the forked posterior process of the ectopterygoid. Posteriorly, each pterygoid bears the long, laterally compressed quadrate process, which constitutes about half the length of the bone. The quadrate process extends posterolaterally to reach the ventral portion of the medial aspect of the quadrate. The anteromedial aspect of each quadrate process contacts the distal end of the basipterygoid process of the parabasisphenoid. Dorsally, the proximal end of each quadrate process bears the columellar fossa, which receives the ventral end of each epipterygoid. There are 14 ossicles in each eye, but their margins are not well resolved in the CT scans.

The dentary is more than half the length of the lower jaw laterally and bears 17 teeth on a well-defined alveolar shelf. Mandibular dentition is heterodont, with small conical anterior teeth and larger, tricuspid (lateral cusps much smaller than the medial one) posterior teeth. Posteriorly, the dentary extends as much as the overlying coronoid. The posterior margin of the dentary articulates with several bones. In lateral view, it articulates with the surangular and is largely overlapped by the labial process of the coronoid. In lingual aspect, the dentary is bifurcate; the ventral splenial process and anteroventral portion of the dorsal coronoid process articulate with the splenial, whereas the posterior aspect of the dorsal coronoid process is overlapped by the anterior lingual process of the coronoid. The dorsolateral margin of the dentary, at its union with the coronoid, lies ventral to the dorsal margin of the surangular. Posteromedially, the dentary articulates with the anterodorsal margin of the angular. Laterally, the anterior half of the dentary bears four mental foramina, which lie in a longitudinal series halfway between the ventral and dorsal margins.

The coronoid lies immediately behind the mandibular tooth row. Its dorsal process is nearly as high as the maximum height of the dentary. Ventrolaterally, the labial process of the coronoid

TABLE 1. Lepidosis and measurements of *Selvasaura almendarizae* sp. nov. and *S. brava*. Data of *S. brava* are based on Moravec et al. (2018).

Character	*Selvasaura almendarizae* sp. nov. ($n = 3$)	*Selvasaura brava* ($n = 6$)
Transverse rows of dorsals between occiput and posterior margin of hindlimb	25–32	33–36
Scales around midbody	29–32	32–34
Lateral scale rows at midbody	5	6–7
Transverse rows of ventrals between collar fold and preanals	20–23	22–25
Longitudinal rows of ventrals at midbody	8–10	10
Scales on collar	7–9	9–11
Subdigital lamellae on finger IV	12–16	14–16
Subdigital lamellae on toe IV	18–20	18–22
Femoral pores in males (one leg)	9–12	7–9
Maximum SVL in males (mm)	39.73	45.9
Maximum SVL in females (mm)	Unknown	42.1

overlaps the dentary posterior to the tooth row. The coronoid articulates posteriorly with the surangular. In medial aspect, the coronoid bears two processes. The anterior lingual process articulates with the dentary anteriorly, splenial ventrally, and prearticular posteriorly. The posterior lingual process overlaps the anteromedial portion of the prearticular. The base of the lingual bifurcation of the coronoid is wide and dorsally concave.

The surangular occupies the posterior half of the mandible and forms the dorsal portion of the lower jaw between the coronoid and articular. It bears a large anterolateral foramen immediately posterior to the articulation with the coronoid and a smaller posterolateral foramen. In lateral aspect, the surangular tapers anteriorly between the coronoid dorsally and dentary ventrally. The ventrolateral border of the surangular articulates anteriorly with the dentary and behind it with the angular. Medially, the surangular bears three large foramina longitudinally aligned along the adductor fossa, followed posteriorly by three much smaller foramina. The surangular is fused with the articular/prearticular complex. The prearticular forms the posterior end of each mandibular ramus and lies mostly on the ventral and lingual aspects of the mandible.

Posteriorly, the prearticular bears the retroarticular process posteriorly and a short, semicircular angular process medially. The latter extends anteriorly as a prominent longitudinal crest, of which the anterior end is overlapped by the posteromedial process of the coronoid. In dorsal view, the retroarticular process is defined by two rounded crests that converge posteriorly, namely, the tympanic crest laterally and the medial crest medially. The medial crest bears the chorda tympani foramen at the medial side of its proximal end. Anterior to the angular and retroarticular processes, the dorsal aspect of the prearticular is fused with the overlying articular.

The angular is a small, slender bone that lies along the ventral surface of each mandibular ramus. Posteriorly, it articulates with the surangular laterally and prearticular medially. Anteriorly, each angular articulates with the dentary laterally and the splenial medially. Each angular is pierced by a small posterior mylohyoid foramen at the level of the anterior end of the adductor fossa.

The splenial lies on the medial aspect of the mandible. Its anterior end and most of its ventral margin articulate with the dentary; it articulates with the angular posteroventrally. Dorsally, the splenial articulates with the anteromedial process of the coronoid anteriorly and the prearticular posteriorly. The anterior end of the splenial is pierced by a large anterior inferior alveolar foramen, followed ventrally by a much smaller anterior mylohyoid foramen.

Neurocranium: The basioccipital lies between the otic capsules and forms the posterior floor of the braincase and the medial portion of the occipital condyle. Its anterior margin articulates broadly with the parabasisphenoid and bears a broad rectangular notch medially. The basioccipital articulates with the prootic anterolaterally and the otoccipital posterolaterally. On each side, the basioccipital has a short, wide ventrolateral process, dorsal to which the foramen rotundum opens.

The supraoccipital forms the posterior roof of the braincase. Its anteriorly concave posterior margin forms the dorsal rim of the foramen magnum. The V-shaped lateral border of the supraoccipital articulates with the prootic anteriorly and the otoccipital posteriorly. The anterodorsal margin of the supraoccipital is separated from the parietal by a gap and bears the processus ascendens medially, which is directed toward the parietal fossa of the parietal. On each side of this process, the dorsal surface of the supraoccipital bears a shallow depression.

Except for its short anteromedial cultriform process, the parasphenoid is fused with the basisphenoid to form the parabasisphenoid, which constitutes the anterior floor of the braincase. It articulates with the basioccipital posteriorly and the prootic posterodorsally. In ventral view, the medial portion of the posterior margin of the parabasisphenoid projects posteriorly as a rectangle that fits into the anteromedial notch of the basioccipital. Anteriorly, the parabasisphenoid bears two ventrolaterally oriented basipterygoid processes, which have expanded distal ends that articulate with the quadrate processes of each pterygoid. Dorsal to each basipterygoid process, the parabasisphenoid bears a short dorsolateral alar process, which articulates with the anteroventral process of the prootic. The posterior aspect of the parabasisphenoid is pierced on each side by the entrance to the Vidian canal and bears a short crista anterior to it, which corresponds to an anterior extension of the crista prootica. The thin and short cultriform process extends anteriorly to a point posterior to the posterior ends of the dentaries.

The otoccipitals form the posterolateral walls of the braincase, lateral margins of the foramen magnum, and lateral portions of the occipital condyle. They meet the prootics anteriorly (suture not visible), supraoccipital dorsally, and basioccipital ventrally. Each otoccipital bears a short lateral paraoccipital process. Two foramina pierce the posterior surface of each otoccipital lateral to the occipital condyle; they are the dorsal hypoglossal foramen ventrally and the vagal foramen dorsally. Anterior to the paraoccipital process, each otoccipital has a deep concavity that corresponds to the posterior portion of the jugular recess. The fenestra ovalis lies mostly in the otoccipital and receives the footplate of the stapes; it lies between the jugular recess and the foramen rotundum. The anterior margin of the fenestra ovalis is formed by the posteroventral margin of the prootic. The crista interfenestralis separates the fenestra ovalis from the foramen rotundum.

The prootics form the anterolateral walls of the braincase. Each prootic bears a large anterodorsally oriented alar process, which articulates with the lateral margin of the supraoccipital posteriorly. The anterior margin of the alar process forms the crista alaris, ventral to which the prootic bears a lateral bulge that corresponds to the acoustic recess medially. The anteroventral process of the prootic articulates with the parabasisphenoid anteriorly and the basioccipital ventrally. The anteroventral process bears ventrally a large cavity that corresponds to the anterior portion of the jugular recess. Ventrolaterally, each prootic bears a conspicuous crista prootica, which constitutes the lateral wall of the jugular recess. The distinct trigeminal notch on the anteroventral aspect of the prootic is formed by the dorsal margin of the anteroventral process and the ventral margin of the alar process. Posteriorly, the prootic overlaps the anterior surface of the paraoccipital process of the otoccipital and forms the anterior margin of the fenestra ovalis. The boomerang-shaped orbitosphenoids lie immediately anterior to the cultriform process and form the lateral margins of the optic foramen.

Splanchnocranium: The quadrates lie on the posterolateral corners of the skull, articulating with and supporting the lower jaw. Ventrally, each quadrate bears a large transverse condyle that articulates with the glenoid fossa of the articular. A prominent crest extends posterodorsally from the transverse condyle to the cephalic condyle that forms the posterodorsal

end of each quadrate. The cephalic condyle articulates with the posterior end of the supratemporal, the posterior end of the squamosal, and the distal end of the paraoccipital process of the otoccipital. Each quadrate is divided into a wide, anterolaterally concave lateral half bearing the tympanic crest along its lateral margin and a short medial half bearing the medial crest along its medial margin. The tympanic crest is notched close to its dorsal end. The medial half of each quadrate is in close contact with the quadrate process of the pterygoid ventromedially.

The rod-shaped epipterygoids form a pair of vertical braces between the palate and the skull table. The ventral end of each epipterygoid inserts into the columellar fossa of the quadrate process of the corresponding pterygoid, whereas the dorsal end surpasses the ventral tip of the ventrolateral extension of the parietal laterally in close distance but without contacting it.

Each thin cylindrical stapes lies anteroventral to the paraoccipital process of the otoccipital and bears an expanded proximal end forming an elongated footplate that attaches to the membrane covering the fenestra ovalis. The articular bone lies on the dorsal aspect of the posterior portion of each mandibular ramus between the proximal portions of both the retroarticular and angular processes of the prearticular, with which it is fused. It is also fused anteriorly with the surangular. It bears a pair of dorsal concavities, the medial and lateral portions of the glenoid fossa, which form the articular facet of the lower jaw.

Color of Holotype.—Based on photographs of a freshly killed specimen, the dorsal surface of head, body, and limbs is light brown with dark-brown or black spots; light-brown vertebral stripe (~2 dorsal scales wide) extending from occiput to tail, finely bordered laterally by dark brown; faint tan dorsolateral line extending on each side from supratympanic scales to shoulder; narrow yellowish cream stripe from mouth commissure, through ventral border of tympanum, to forelimb insertion, and extending posteriorly as a ventrolateral band that fades away before reaching hindlimb; sides of neck and flanks light brown; one conspicuous ocellus with thick black border and cream center above forelimb insertion, followed by 3/2 (right/left) ocelli on flanks posteriorly; tail orange ventrally and reddish brown laterally; throat light olive green with brass tint and dispersed black dots; venter olive green with dark marks within each scale.

In preservative, dorsal surface of head and body gray, limbs whitish brown with scattered black markings, dorsal surface of tail light brown; vertebral stripe light gray becoming light brown toward the tail, bordered laterally by scattered black marks; flanks light gray with bronze-brown tint, ocelli on shoulders and flanks as described above; throat and belly creamy white with black spots; ventral surfaces of limbs and tail yellowish white (Fig. 1).

Color in Life of Paratype QCAZ 9140.—Dorsal surface of head, body, and limbs light brown with dark-brown spots; cream vertebral stripe extending from occiput to tail, bordered laterally by fine dark brown; nearly inconspicuous tan dorsolateral line extending on each side from supratympanic scales to hindlimbs; narrow white stripe bordered by dark brown dorsally extending from below orbit to forelimb insertion; sides of neck and flanks light brown; nine ocelli-like spots along flanks, from neck to hindlimb insertion; tail flanks light brown with orange tint; throat creamy white; chest and belly creamy white with light green tint, and fine dark-green and cream spots on individual scales; ventral surface of forelimbs light brown; ventral surface of hindlimbs and cloacal plate yellowish white; ventral surface of tail creamy white, with scattered orange marks; iris orange (Fig. 6).

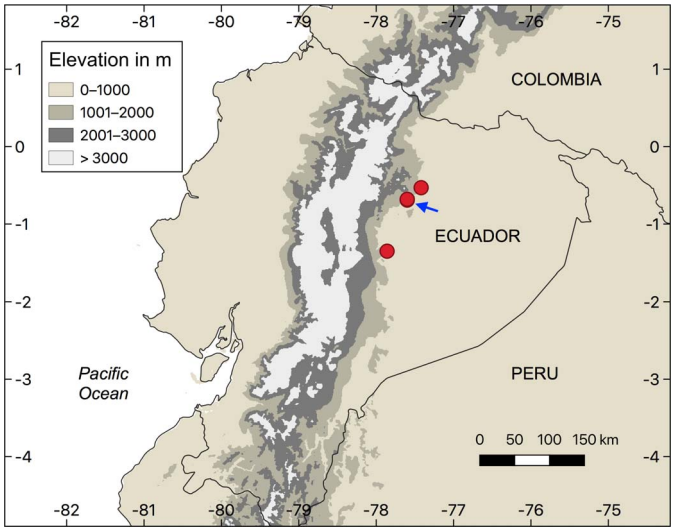

FIG. 9. Distribution of *Selvasaura almendarizae* sp. nov. in Ecuador. Arrow points at type locality. The northernmost locality is based on the photographs presented in Fig. 6C,D.

Hemipenis of Paratype QCAZ 5073.—Organ partially everted and partially expanded, 4–5 mm long (~four subcaudals); organ unilobed, partially damaged during eversion; sulcus spermaticus broad and shallow throughout the hemipenial body, originating at the base of the hemipenis, and extending in a straight line until it divides into 2 branches at the distal 3rd of the organ; sulcal branches separated by fleshy fold; hemipenial body with 14 pairs of chevron-shaped flounces, separated by a longitudinal nude area on asulcate face (except first, proximalmost flounce), with vertices directed proximally on the lateral aspects of the body; flounces ornamented with calcified spicules (Fig. 7).

Other Variation.—Variation in lepidosis and measurements in *Selvasaura almendarizae* sp. nov. is presented in Table 1.

Etymology.—The specific name is a noun in the genitive case and is a patronym for Ana Almendáriz, former curator of Herpetology in the Museo de Historia Natural Gustavo Orcés at Escuela Politécnica Nacional del Ecuador. Ana Almendáriz is an Ecuadorian herpetologist who has made important contributions to the study of amphibians and reptiles from Ecuador including more than a dozen species descriptions. For more than three decades, she also has trained many young herpetologists.

Distribution and Natural History.—*Selvasaura almendarizae* sp. nov. is known from three localities along the northeastern slopes of the Andes of Ecuador at elevations between 950–1,350 m (Fig. 9). This distribution range corresponds to Napo and Pastaza provinces in Ecuador. All specimens were found active during the day. Paratype QCAZ 9140 was found on mainland forest, on a leaf 100 cm above the ground, close to a stream. The new species occurs in Eastern Montane and Eastern Foothill forests (Fig. 10), with annual mean temperatures of 7.2–21.9°C and 20–23.9°C, respectively (Ron, 2017). The type locality of *S. almendarizae* sp. nov. is part of Wildsumaco Wildlife Sanctuary, a 500-ha private reserve located near the Gran Sumaco Biosphere Reserve. The other two localities where this species has been recorded (Fig. 9) also lie within protected areas, indicating that at least some populations of *S. almendarizae* sp. nov. are protected.

Phylogenetic Relationships.—Data partitions and evolution models are presented in Table 2. BI and ML analyses resulted in similar topologies, with only minor discrepancies among poorly supported nodes (Fig. 8; Supplementary Tree Files 1, 2). Monophyly of

FIG. 10. Habitat of the type locality of *Selvasaura almendarizae* sp. nov. at Wildsumaco Wildlife Sanctuary, Napo Province, Ecuador. Photograph by J. D. Camper.

Selvasaura is strongly supported (PP = 1, BS = 92). The sister taxon of *Selvasaura* is a clade (PP = 0.9, BS = 86) composed of *Potamites* and *Dendrosauridion*; however, this relationship is better supported by BI than ML analysis (PP = 0.96 and BS = 49, respectively). The ML analysis placed the new species as a sister to all other congenerics with low support, whereas relationships among species of *Selvasaura* were not resolved by the Bayesian analysis. Both BI and ML analyses maximally support the monophyly of *S. almendarizae* sp. nov., *S. brava*, and an undescribed species of *Selvasaura* from Peru. Mean genetic distances between *S. almendarizae* sp. nov. and *S. brava* are 0.07 (12S) and 0.05 (16S).

DISCUSSION

In this paper, we describe a new species of *Selvasaura*, a genus-ranked clade of Cercosaurinae lizards that was discovered only five years ago (Torres-Carvajal et al., 2016) and described more recently (Moravec et al., 2018). Additionally, our results support the previous recognition of two putative species of *Selvasaura*. One of them is represented by one sample (QCAZ 12891) collected in southeastern Ecuador. Because this sample is the only known sample of this putative new species to date, we refrained from describing it until more material becomes available. The second putative species of *Selvasaura* is from the San Martin region in Peru and is currently being described (see Note Added in Proof below). The monophyly of *Selvasaura* is strongly supported, but its phylogenetic position within Cercosaurinae is less clear. Although *Selvasaura* was originally recovered as a sister to *Potamites* (Torres-Carvajal et al., 2016; Moravec et al., 2018), our results are in agreement with more recent studies (Fang et al., 2020; Vásquez-Restrepo et al., 2020) in that the sister taxon of *Selvasaura* is a clade composed of *Potamites* and the recently discovered *Dendrosauridion* (Fig. 8). All three taxa represent a cis-Andean radiation of Cercosaurinae lizards, and except widespread *Potamites ecpleopus*, they are restricted to extreme western Amazonia and adjacent Andean slopes in southern Colombia, Ecuador, Peru, and Bolivia.

We also present a detailed description of the skull of *S. almendarizae* sp. nov. by using micro-CT scanning. Despite its great diversity and large museum collections for some taxa, the cranial osteology of Cercosaurinae has been described in detail only for a handful of species (Montero et al., 2002; Bell et al., 2003). Notably, Bell et al. (2003) described in detail the cranial osteology of *P. ecpleopus*, which is closely related to *Selvasaura* (Fig. 8). The skull of *S. almendarizae* sp. nov. is similar to that of *P. ecpleopus* in having nasals partially separated by broad dorsal process of premaxilla; frontal narrow, with a trifurcate anterior margin and well-developed cristae cranii that meet ventrally to create tubular structure; maxilla with wide medial shelf that overlaps vomer to separate vomeronasal opening from choana; posterior marginal teeth tricuspid; postfrontal quadriradiate; vomers partially fused; splenial small, beneath rear of tooth row; and in lacking a lacrimal in adults (Fig. 3–5). Some features like tricuspid maxillary teeth and absence of lacrimal have also been reported in other Cercosaurinae taxa, such as *Cercosaura* and *Riama* (Bell et al., 2003). Nonetheless, the lack of information for most major taxa precludes a better understanding of variation in skull morphology among Cercosaurinae lizards, the most diverse clade of South American gymnophthalmid lizards.

TABLE 2. Data partitions used in phylogenetic analyses. Numbers in parentheses indicate codon position. Number of sites, selected model, number of unique site patterns (USP), variable sites (VS), and parsimony-informative sites (PIS) are indicated.

Partition	Sites	Model	USP	VS	PIS
12S, 16S	946	GTR+I+G	586	473	372
ND4 (1)	207	GTR+I+G	145	134	107
ND4 (2)	207	GTR+I+G	77	67	47
ND4 (3)	207	GTR+G	207	207	207
c-mos (3)	128	K80+G	116	100	74
c-mos (1, 2)	254	HKY+G	141	101	63
All	1,949	—	1,272	1,082	870

Acknowledgments.—Special thanks to L. Mahler, University of Toronto, for providing access to the high resolution micro-CT scanner and J. Ortega for scanning the skull described here. J. D. Camper kindly shared photographs of the freshly killed holotype and the type locality habitat, and J. Carrión took photographs of the holotype. This manuscript benefited from critical reviews by T. Doan and an anonymous reviewer. Field and laboratory work were funded by a grant from SENESCYT (Arca de Noé Initiative; S. R. Ron and O. Torres-Carvajal principal investigators). OT-C was also supported by a scholarship from the German Academic Exchange Service (DAAD), and PMSN was supported by Conselho Nacional de Desenvolvimento Científico e Tecnológico - CNPq (fellowship number 313622/2018-3). Specimens were collected under research permits 020-07 IC-FAU-DNBAPVS/MA, 001-11 IC-FAU-DNB/MA, 005-14 IC-FAU-DNB/MA, and MAE-DNB-CM-2015-0025 issued by Ministerio de Ambiente de Ecuador.

NOTE ADDED IN PROOF

While this paper was in press, Echevarría et al. (2021) described *Selvasaura evasa* from northern Peru. These authors provide morphological comparisons between *S. evasa* and both *S. brava* and *S. almendarizae*, to which they refer as "*Selvasaura* sp. Ecuador."

LITERATURE CITED

BELL, C. J., S. E. EVANS, AND J. A. MAISANO. 2003. The skull of the gymnophthalmid lizard *Neusticurus ecpleopus* (Reptilia: Squamata). Zoological Journal of the Linnean Society 139:283–304.

CASTOE, T. A., T. M. DOAN, AND C. L. PARKINSON. 2004. Data partitions and complex models in Bayesian analysis: The phylogeny of gymnophthalmid lizards. Systematic Biology 53:448–469.

CHÁVEZ, G., A. CATENAZZI, AND P. J. VENEGAS. 2017. A new species of arboreal microteiid lizard of the genus *Euspondylus* (Gymnophtalmidae: Cercosaurinae) from the Andean slopes of central Peru with comments on Peruvian *Euspondylus*. Zootaxa 4350:301–316.

DE QUEIROZ, K. 2007. Species concepts and species delimitation. Systematic Biology 56:879–886.

ECHEVARRÍA, L. Y., P. J. VENEGAS, L. A. GARCÍA-AYACHI, AND P. M. S. NUNES. 2021. An elusive new species of gymnophthalmid lizard (Cercosaurinae, *Selvasaura*) from the Andes of northern Peru. Evolutionary Systematics 5:177–187.

EVANS, S. E. 2008. The skull of lizards and tuatara. Pp. 1–347 in C. GANS, A.S. GAUNT, AND K. ADLER (eds.), Biology of the Reptilia, Vol. 20 Morphology H: The Skull of Lepidosauria. Society for the Study of Amphibians and Reptiles, Ithaca, NY, USA.

FANG, J. M., J. D. VÁSQUEZ-RESTREPO, AND J. M. DAZA. 2020. Filling the gaps in a highly diverse Neotropical lizard lineage: a new and endemic genus of Cercosaurinae (Squamata: Gymnophthalmidae) with the description of two new species from the Northern Andes of Colombia. Systematics and Biodiversity 18:417–433.

GOICOECHEA, N., D. R. FROST, I. DE LA RIVA, K. C. M. PELLEGRINO, J. SITES JR., M. T. RODRIGUES, AND J. M. PADIAL. 2016. Molecular systematics of teioid lizards (Teioidea/Gymnophthalmoidea: Squamata) based on the analysis of 48 loci under tree-alignment and similarity-alignment. Cladistics 32:624–671.

HARVEY, M. B., AND D. EMBERT. 2008. Review of Bolivian *Dipsas* (Serpentes: Colubridae), with comments on other South American species. Herpetological Monographs 22:54–105.

HERNÁNDEZ MORALES, C., M. J. STURARO, P. M. S. NUNES, S. LOTZKAT, AND P. L. V. PELOSO. 2020. A species-level total evidence phylogeny of the microteiid lizard family Alopoglossidae (Squamata: Gymnophthalmoidea). Cladistics 36:301–321.

KUMAR, S., G. STECHER, AND K. TAMURA. 2016. MEGA7: molecular evolutionary genetics analysis version 7.0 for bigger datasets. Molecular Biology and Evolution 33:1870–1874.

LANFEAR, R., B. CALCOTT, S. Y. W. HO, AND S. GUINDON. 2012. PartitionFinder: Combined selection of partitioning schemes and substitution models for phylogenetic analyses. Molecular Biology and Evolution 29:1695–1701.

LEHR, E., J. MORAVEC, M. LUNDBERG, G. KÖHLER, A. CATENAZZI, AND J. ŠMÍD. 2019. A new genus and species of arboreal lizard (Gymnophthalmidae: Cercosaurinae) from the eastern Andes of Peru. Salamandra 55: 1–13.

MANZANI, P. R., AND A. S. ABE. 1988. Sobre dois novos métodos de preparo do hemipenis de serpentes. Memorias do Instituto Butantan (São Paulo) 50:15–20.

MONTANUCCI, R. R. 1973. Systematics and evolution of the Andean lizard genus *Pholidobolus* (Sauria: Teiidae). University of Kansas Museum of Natural History, Miscellaneous Publications 59:1–52.

MONTERO, R., S. A. MORO, AND V. ABDALA. 2002. Cranial anatomy of *Euspondylus acutirostris* (Squamata: Gymnophthalmidae) and its placement in a modern phylogenetic hypothesis. Russian Journal of Herpetology 9:215–228.

MORAVEC, J., J. ŠMÍD, J. ŠTUNDL, AND E. LEHR. 2018. Systematics of Neotropical microteiid lizards (Gymnophthalmidae, Cercosaurinae), with the description of a new genus and species from the Andean montane forests. ZooKeys 774:105–139.

NUNES, P. M. S. 2011. Morfologia Hemipeniana dos Lagartos Microteídeos e Suas Implicações nas Relações Filogenéticas da Família Gymnophthalmidae (Squamata: Teiioidea). Ph.D., Universidade de São Paulo, Brazil.

NUNES, P. M. S., A. FOUQUET, F. F. CURCIO, P. J. R. KOK, AND M. T. RODRIGUES. 2012. Cryptic species in *Iphisa elegans* Gray, 1851 (Squamata: Gymnophthalmidae) revealed by hemipenial morphology and molecular data. Zoological Journal of the Linnean Society 166:361–376.

PARRA, V., P. M. S. NUNES, AND O. TORRES-CARVAJAL. 2020. Systematics of *Pholidobolus* lizards (Squamata, Gymnophthalmidae) from southern Ecuador, with descriptions of four new species. ZooKeys 954:109–156.

PELLEGRINO, K. C. M., M. T. RODRIGUES, Y. YONENAGA-YASSUDA, AND J. W. SITES. 2001. A molecular perspective on the evolution of microteiid lizards (Squamata, Gymnophthalmidae), and a new classification for the family. Biological Journal of the Linnean Society 74:315–338.

PESANTES, O. S. 1994. A method for preparing the hemipenis of preserved snakes. Journal of Herpetology 28:93–95.

RAMBAUT, A. 2018. FigTree version 1.4, Available from: http://tree.bio.ed.ac.uk/software/figtree/.

RAMBAUT, A., A. J. DRUMMOND, D. XIE, G. M.BAELE, AND A. SUCHARD. 2018. Posterior summarization in Bayesian phylogenetics using Tracer 1.7. Systematic Biology 67:901–904.

RECODER, R., I. PRATES, S. MARQUES-SOUZA, A. CAMACHO, P. M. S. NUNES, F. DAL VECHIO, J. M. GHELLERE, R. W. MCDIARMID, AND M. T. RODRIGUES. 2020. Lizards from the Lost World: two new species and evolutionary relationships of the Pantepui highland *Riolama* (Gymnophthalmidae). Zoological Journal of the Linnean Society 190:271–297.

RON, S. R. 2017. Regiones naturales del Ecuador. BIOWEB. Pontificia Universidad Católica del Ecuador. Available from: https://bioweb.bio/faunaweb/reptiliaweb/RegionesNaturales.

RONQUIST, F., M. TESLENKO, P. VAN DER MARK, D. L. AYRES, A. DARLING, S. HÖHNA, B. LARGET, L. LIU, M. A. SUCHARD, AND J. P. HUELSENBECK. 2012. MrBayes 3.2: efficient Bayesian phylogenetic inference and model choice across a large model space. Systematic Biology 61:539–542.

SÁNCHEZ-PACHECO, S. J., O. TORRES-CARVAJAL, V. AGUIRRE-PEÑAFIEL, P. M. S. NUNES, L. VERRASTRO, G. A. RIVAS, M. T. RODRIGUES, T. GRANT, AND R. W. MURPHY. 2018. Phylogeny of *Riama* (Squamata: Gymnophthalmidae), impact of phenotypic evidence on molecular datasets, and the origin of the Sierra Nevada de Santa Marta endemic fauna. Cladistics 34:260–291.

STAMATAKIS, A. 2014. RAxML version 8: a tool for phylogenetic analysis and post-analysis of large phylogenies. Bioinformatics 30:1312–1313.

TORRES-CARVAJAL, O. 2003. Cranial osteology of the Andean lizard *Stenocercus guentheri* (Squamata: Tropiduridae) and its postembryonic development. Journal of Morphology 255:94–113.

TORRES-CARVAJAL, O., S. E. LOBOS, P. J. VENEGAS, G. CHÁVEZ, V. AGUIRRE-PEÑAFIEL, D. ZURITA, AND L. Y. ECHEVARRÍA. 2016. Phylogeny and biogeography of the most diverse clade of South American gymnophthalmid lizards (Squamata, Gymnophthalmidae, Cercosaurinae). Molecular Phylogenetics and Evolution 99:63–75.

UETZ, P., P. FREED, AND J. HOŠEK. 2020. The Reptile database. Available from: http://www.reptile-database.org.

UZZELL, T. M. 1973. A revision of lizards of the genus *Prionodactylus*, with a new genus for *P. leucostictus* and notes on the genus *Euspondylus* (Sauria, Teiidae). Postilla 159:1–67.

VÁSQUEZ-RESTREPO, J. D., R. IBÁÑEZ, S. J. SÁNCHEZ-PACHECO, AND J. M. DAZA. 2020. Phylogeny, taxonomy and distribution of the Neotropical lizard genus *Echinosaura* (Squamata: Gymnophthalmidae), with the recognition of two new genera in Cercosaurinae. Zoological Journal of the Linnean Society 189:287–314.

ZAHER, H. 1999. Hemipenial morphology of the South American xenodontine snakes, with a proposal for a monophyletic Xenodontinae and a reappraisal of colubroid hemipenes. Bulletin of the American Museum of Natural History 240:1–168.

Accepted: 14 April 2021.
Published online: 27 September 2021.

SUPPLEMENTARY DATA

Supplementary data associated with this article can be found online at http://dx.doi.org/10.1670/20-142.